Heterogeneously flagellated microswimmer behavior in viscous fluids ⓢ Ⓕ

View Online   Export Citation   CrossMark

Louis William Rogowski, ⓘ Micah Oxner, ⓘ Jiannan Tang, ⓘ and Min Jun Kim[a]) ⓘ

AFFILIATIONS

Department of Mechanical Engineering, Southern Methodist University, 3101 Dyer Street, Suite 200, Dallas, Texas 75206, USA

[a])Author to whom correspondence should be addressed: mjkim@lyle.smu.edu

ABSTRACT

An analysis of heterogeneously flagellated microswimmers inside viscous fluids is presented. Flagella harvested from *Salmonella typhimurium* were isolated, repolymerized, and functionalized to have biotin at their ends, allowing for chemical attachment along the surfaces of avidin-coated microparticles. Assembled microswimmers were rotated under incremental magnetic field frequencies, in saline and methylcellulose solutions, to baseline their velocity responses. A mean square displacement analysis revealed that rotating microswimmers exhibited anomalous diffusive behavior at small time scales in each fluid and had increased diffusivity compared with the non-rotating cases. Flagellated microswimmers had decreased diffusivity when compared with non-flagellated microparticles in Brownian conditions. Microswimmers were demonstrated to perform selected trajectories under proportional feedback control with reasonable accuracy. Finally, microswimmer propulsion was shown to be heavily influenced by the handedness of the rotating magnetic fields, with frequency induced reversals of swimming direction observed under clockwise rotation; this effect was determined to be the result of flagellar bundling and unbundling.

I. INTRODUCTION

Microrobots are promised to be instrumental in the future of medicine, being poised to lead advances in minimally invasive surgery, targeted drug delivery, and *in vivo* diagnostics. Microrobotic propulsion methods are often limited by the low Reynolds number regime, where viscous forces dominate, thus requiring nonreciprocal strokes or nonreciprocal actuation methods to propel.[1,2] Several microrobots, which rely on helices to generate nonreciprocal strokes, were developed using direct laser writing (DLW) methods[3,4] and were demonstrated to perform cargo transport applications.[5–13] Other helical based microrobots have been assembled through templating organic geometries[14–16] and polymers,[17,18] while countless other microrobots have been developed to achieve meaningful propulsion utilizing catalytic propulsion,[19,20] nonreciprocal actuation of magnetic microparticle aggregates,[21,22] and acoustic actuation.[23] While all of these microrobots are impressive in their own right, there exists a need for a microrobot that can be assembled quickly and adapted to operate within diverse fluidic environments. The rotation and bundling of flagellar filaments are the primary means of locomotion by several types of bacteria;[24] flagellin subunits, which make up the flagellar filaments, are naturally self-assembling and can

polymorphically transform[25,26] based on external stimuli such as pH,[27] physical stress,[28] and physiochemical changes within the surrounding environment.[29] Utilizing these flagella to create simple and efficient artificial microswimmers will allow for environmental adaptation and sensing. Without the onboard motors commonly found in bacteria, flagella have to be chemically attached to magnetic microparticles so that they can be rotated using externally applied magnetic fields; these fields induce a torque analogous to the ones produced by the onboard motors. Microparticles by themselves are incapable of propelling by pure rotation within Newtonian fluids, since they lack the flexibility and chirality necessary for propulsion in low Reynolds number environments.[1,2,30] The addition of a flagellar surface coating breaks the symmetry of the microparticle and allows for meaningful propulsion when exposed to rotating magnetic fields.

Significant research has already been done documenting the isolation and repolymerization of bacterial flagella,[31,32] and in previous work, polymorphic transformations were induced to understand how nanoswimmers, attached with a single flagellum, propelled using different coil forms.[33] These same nanoswimmers were also templated with nickel and titanium to improve

responsiveness to applied magnetic fields and demonstrate bio-compatibility.[34] Bacteria-inspired dumbbell microswimmers were fabricated by linking a microparticle with a magnetic nanoparticle using a flagellar filament.[35] As opposed to having a single flagellum attached to a magnetic microparticle, a surface coating of flagella can be more advantageous, allowing for fast reliable fabrication of microswimmers and enabling diverse motion modes. The work presented here will investigate the propulsion characteristics of microswimmers formed by functionalizing 2 μm diameter magnetic microparticles with a surface coating of flagellar filaments. These microswimmers were investigated for their responsiveness to rotational magnetic field actuation, their comparative performance in Newtonian solutions of different viscosity, their ability to perform simple trajectories, and their unique motion modes that occurred as a function of applied magnetic field rotation handedness. An illustration of the fabrication process for the microswimmers can be seen in Figs. 1(a)–1(k), with select heterogeneously flagellated microswimmers shown in Figs. 1(l)–1(o). The experimental setup [Fig. 1(p)] and the magnetic field strength vs frequency ratio used for these experiments [Fig. 1(q)] are also provided. The processes associated with Fig. 1 are elaborated further in Sec. IV.

II. RESULTS

A. Generalized microswimmer performance

For this study, microswimmers were suspended inside 30% NaCl, 0.2% methylcellulose, and 0.4% methylcellulose solutions; microswimmers were then actuated at different rotational frequencies to generate generalized velocity profiles for each medium. The 30% NaCl solution was used to create a neutrally buoyant fluid medium for the microswimmers and replicate an environment similar to water. Methylcellulose solutions are well known polymer fluids, which increase in viscosity as concentration increases;[36,37] while methylcellulose is known to exhibit non-Newtonian shear thinning behavior at high shear rates, under low shear rates, it maintains a Newtonian plateau.[36] For the purposes of these experiments, microswimmers were only operated within the Newtonian regime. Using documentation from Sigma Aldrich, the viscosities were estimated to be approximately 9 and 19 centipoise (cP) for
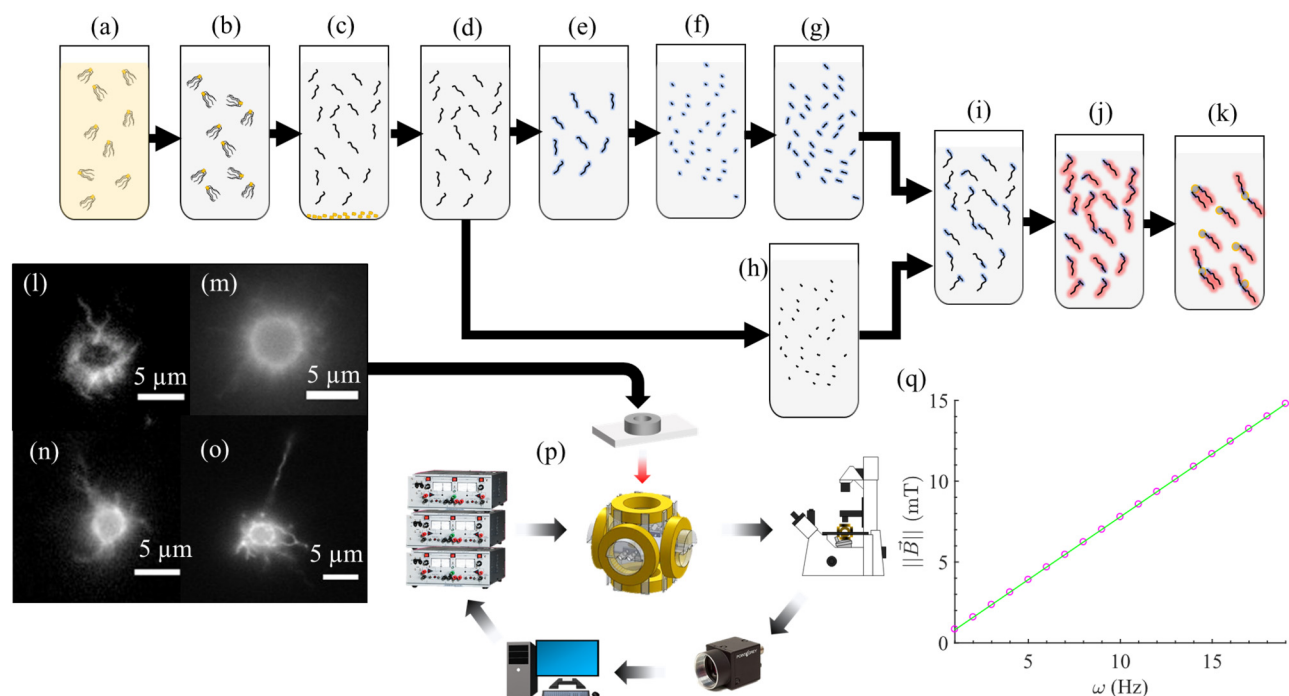
FIG. 1. (a) *S. typhimurium* were concentrated from a 10 L culture medium into a single solution through repeated centrifugation and resuspension. (b) *Salmonella* were pelleted and resuspended in polymerization buffer. (c) Flagella were sheared from the bacterial bodies and bacterial bodies were pelleted through centrifugation. (d) Flagella were purified through centrifugation. (e) About 20% of flagella were separated and coated with a NHS-Biotin complex. (f) Biotinylated flagella and (h) non-biotinylated flagella were depolymerized into flagellin monomers. (g) Biotinylated flagella were concentrated into seeding particles. (i) Biotinylated seeding particles were combined with non-biotinylated flagellin monomers and repolymerized into long flagella with biotinylated tips. (j) Flagella were fluorescently labeled using Cy3 dye. (k) Avidin-coated iron oxide particles (2 μm diameter) were introduced and chemically combined with flagella to form microswimmers. (l)–(o) Microswimmers with different distributions of flagella captured by an electron-multiplying charge-coupled device (EMCCD) camera; entire surfaces of microparticles were usually coated with flagella, with the average length of flagella along the surfaces being approximately 8 μm. (p) Overview of experimental setup, with approximate Helmholtz coil systems and computer controlled power supplies that respond to feedback from a camera. (q) Total magnetic field strength graph and its relationship to frequency used during experiments ($B_r = 0.5\omega$).

0.2% and 0.4% methylcellulose concentrations, respectively. The density of the methylcellulose solutions was high enough to allow microswimmers to remain suspended in solution for prolonged periods of time without noticeable gravity-driven sedimentation. The viscosity of the 30% NaCl solution was assumed to be ∼1 cP from literature.[38] Prior to experiments, litmus paper was used to verify that each solution had a neutral pH (∼7) to ensure flagellar polymorphic changes did not occur as a result of fluid properties and that all flagella remained normal form in solution. From previous work, flagella were not observed to change coil forms through shear stress during magnetic actuation.[33] Since flagella often coated the entire microparticle surface, the exact number of flagella (short and long) was difficult to visually determine; however, through visual estimation, there were usually 12–24 long flagella on each microswimmer, with each having an average length of approximately $8\,\mu m$.

The equations governing the magnetic fields used to rotate the microswimmers were

$$\vec{B} = \begin{bmatrix} -B_s \cos\theta + B_r \sin\theta \cos\omega t \\ B_s \sin\theta + B_r \cos\theta \cos\omega t \\ B_r \sin\omega t \end{bmatrix}, \qquad (1)$$

$$\vec{n} = [-\cos\theta \sin\theta \, 0], \qquad (2)$$

where $\vec{B}$ is the magnetic field vector, B_r is the maximum amplitude of the rotating magnetic field, B_s is the amplitude of the static magnetic field, ω is the rotational frequency of the field, θ is the heading angle, t is the time, and $\vec{n}$ is the direction vector. Dipoles of the microswimmer aligned with $\vec{B}$ as it rotated in the plane perpendicular to the direction vector ($\vec{n}$); propulsion along $\vec{n}$ indicated swimming was occurring. The static field, B_s, imparted a small precision angle that offsets the magnetic field vector (and the dipoles) from the rotation plane perpendicular to the heading vector. Looking from behind the heading vector, the handedness of rotation about it can be treated as either clockwise or counterclockwise, causing the microparticles' dipoles to follow in tandem. Due to the random surface distributions of flagella, microswimmers would either propel positively or negatively along $\vec{n}$; however, this could be modulated by changing the amplitude of B_s from positive to negative. Using Eqs. (1) and (2), microswimmers were subjected to increasing rotational magnetic field frequency and propelled along the positive x-direction; any microswimmers propelling opposite this direction were either modulated to swim in the correct direction using the static field or the velocity profile was adjusted in postprocessing to have the correct sign. For all experiments, B_s was fixed at a constant value (± 0.2 mT), ω was increased at 1 Hz increments, θ was fixed at zero degrees, $\vec{B}$ was rotated in the counterclockwise direction, and both B_r and $\|\vec{B}\|$ increased linearly with increasing ω ($B_r = 0.5\omega$); a graph of the relationship for $\|\vec{B}\|$ to ω can be seen in Fig. 1(q). The results of these rotation experiments produced the velocity vs frequency curves found in Fig. 2.

The velocity of microswimmers suspended in 30% NaCl increased linearly with frequency. Microswimmers tested inside the 0.2% methylcellulose solution experienced a consistent velocity lag at frequencies below 5 Hz, causing velocity to plateau; beyond this

critical point of 5 Hz, the velocity of the microswimmers increased linearly with frequency. The 0.4% microswimmers had a linear relationship along the frequency range, but their overall velocity was greatly reduced. The cause of the velocity lag in 0.2% methylcellulose microswimmers was speculated to be the result of the fluids increased viscosity and possible hindrances from polymer fibers at frequencies below 5 Hz (at this concentration). After this critical point, the slope of the 0.2% methylcellulose microswimmers velocity profile suggests that if frequencies were to continue to increase, they would overtake the speeds of the microswimmers in the 30% NaCl fluid. The most likely reason for this improved performance is increased interaction with polymer fibers at higher rotational frequencies, with similar performance increases documented in other polymer fluids of low concentration by both micro-organisms and artificial microswimmers.[39–44] To ensure microswimmer propulsion was the result of flagellar coatings, velocity vs frequency curves for non-flagellated microparticles were also produced. Microswimmers and microparticles rotated in each medium can be seen in Figs. 2(b)–2(d) for 30% NaCl, 0.2% methylcellulose, and 0.4% methylcellulose, respectively. Microparticles displayed no velocity relationship with increasing frequency in any of the fluids, with the near constant residual velocity observed from the microparticles being the result of a slight drift in the fluids caused from external disturbances. From this, it can be concluded that only microswimmers (microparticles with flagellar coatings) could actively propel inside each fluid medium.

B. Mean square displacement analysis

To complement the results of Sec. II A, a two-dimensional mean squared displacement analysis was performed to analyze the behavior of microswimmers under rotating and non-rotating cases. The mean square displacement (MSD) was calculated using

$$\langle r_\tau^2 \rangle = \frac{1}{N-\tau} \sum_{i=1}^{N-\tau} [r(t_i + \tau) - r(t_i)]^2, \qquad (3)$$

where $\langle r_\tau^2 \rangle$ is the MSD, N is the number of time steps for a given trajectory, τ is the lag time, r is the position vector, and t_i is the ith time increment.[45] For both the rotating and non-rotating cases the MSD profiles were modeled using

$$\langle r_\tau^2 \rangle \propto 4D\tau^\alpha, \qquad (4)$$

where D is generalized diffusion and α is the anomalous diffusion exponent; fittings were produced from the ensemble averaged MSD data over multiple rotating microswimmers (at least three microswimmers per fluid medium with at least three trials each) and non-rotating microswimmers (dozens of individual microswimmers per fluid). Microswimmers were rotated at 19 Hz, while no externally applied magnetic field (static or rotating) was applied during the non-rotating cases. The N for Eq. (3) was at least 600 for all trials. The smallest increment of τ was 1/30th of a second. The lag time intervals over which the nonlinear fittings were performed for rotating and non-rotating cases were different; the time interval for the rotating case was between 2 and 5 s, while for the non-rotating case,
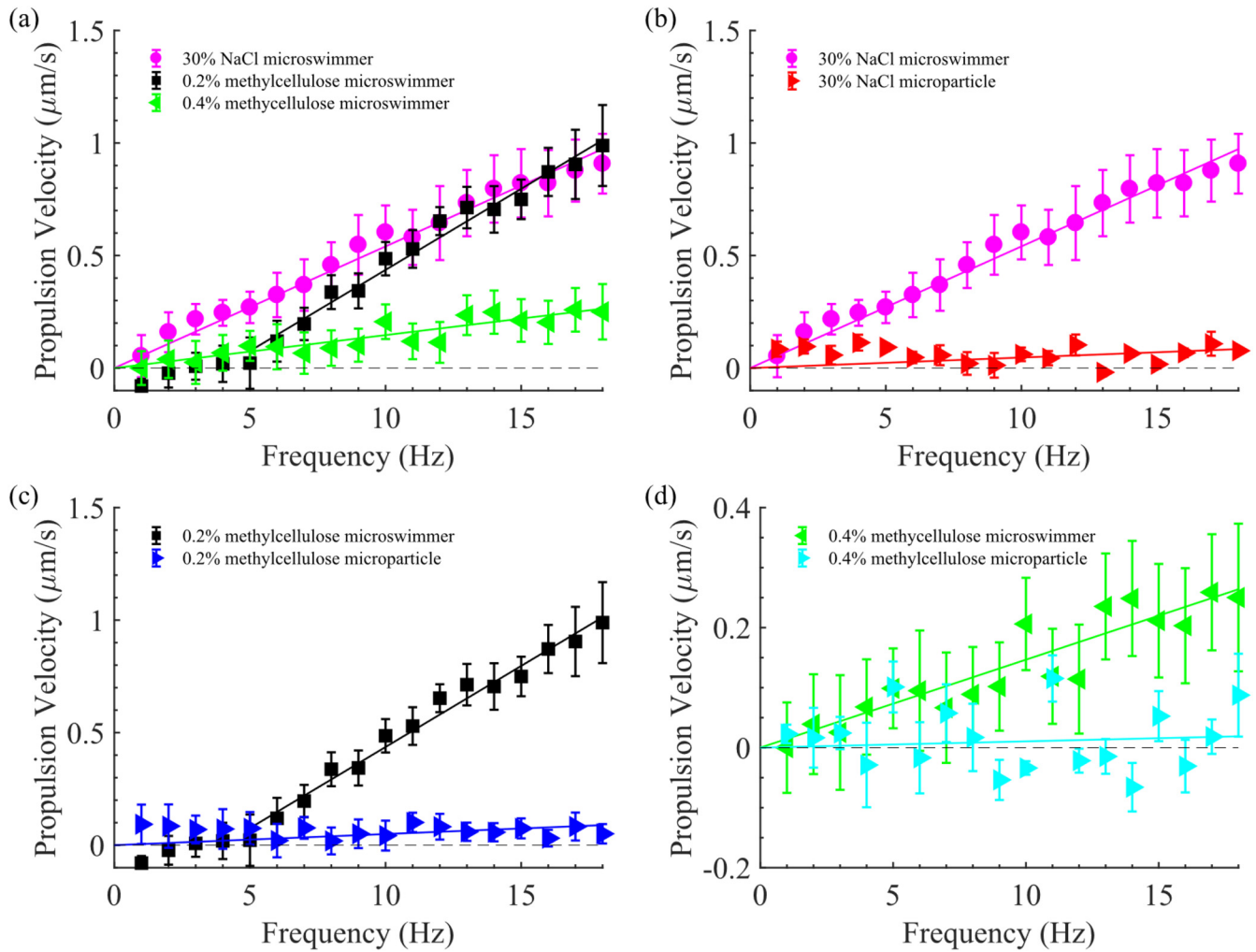
FIG. 2. (a) Propulsion velocity vs frequency curves for microswimmers in different fluid mediums. Microswimmers were compared with non-flagellated microparticles under the same frequency range in (b) 30% NaCl, (c) 0.2% methylcellulose, and (d) 0.4% methylcellulose. Error bars represent the standard error.

the interval was between 1/30th of a second and 3 s. These intervals were chosen because the rotating cases tended to become homogeneous in this range and the non-rotating cases tended to display unreliable behavior at larger lag times. A delayed rejection adaptive Metropolis (DRAM) Markov chain Monte Carlo technique was utilized to estimate the coefficients of Eq. (4) for both rotating and non-rotating cases (see Sec. IV).[46] The parameters estimated using this technique can be found in Table I and the results of the experiments can be visually seen in Fig. 3 for both the rotating and non-rotating cases.

The behavioral differences between rotating and non-rotating microswimmers can be seen in Figs. 3(a)–3(c) for (a) 30% NaCl, (b) 0.2% methylcellulose, and (c) 0.4% methylcellulose, respectively.

TABLE I. Coefficients for Fig. 3.

Test	ω (Hz)	$D\left(\frac{\mu m^2}{s^\alpha}\right)$	α
30% NaCl microswimmer	19	1.16	1.98
30% NaCl microswimmer	0	0.021	0.99
30% NaCl microparticle	0	0.0256	0.97
0.2% MC microswimmer	19	0.21	1.87
0.2% MC microswimmer	0	0.0096	0.97
0.2% MC microparticle	0	0.0127	0.93
0.4% MC microswimmer	19	0.0418	1.86
0.4% MC microswimmer	0	0.0033	0.99
0.4% MC microparticle	0	0.0029	0.88
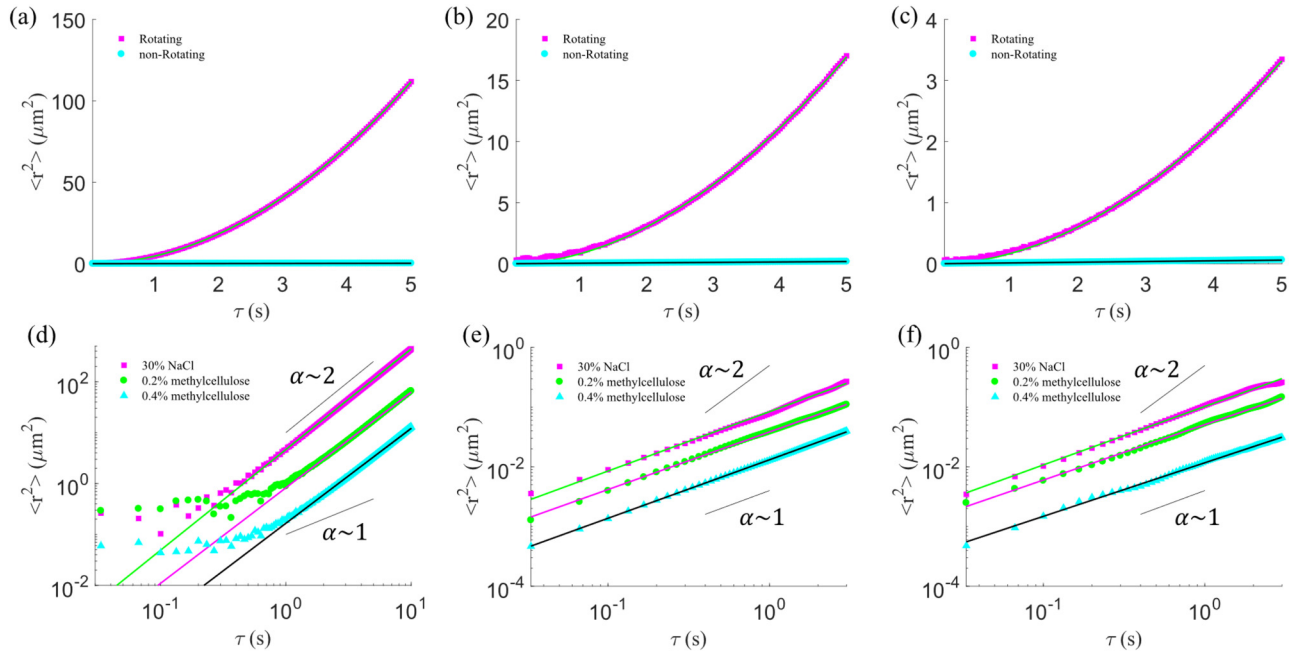
FIG. 3. (a)–(c) Mean square displacement curves for microswimmers in (a) 30% NaCl, (b) 0.2% methylcellulose, and (c) 0.4% methylcellulose under both rotating (19 Hz) and non-rotating cases. (d) The mean square displacement of the rotating microswimmers from all three fluid mediums. (e) Mean square displacement of non-rotating microswimmers in each fluid medium. (f) Mean square displacement of non-rotating microparticles (non-flagellated) in all three mediums. The contrasting solid colored lines represent the fits produced from the coefficients estimated in Table I; in (a)–(f), the green, magenta, and black solid lines correspond to the magenta, green, and cyan data points, respectively. Short solid black lines in (d)–(f) represent curves showing superdiffusion ($\alpha > 1$) and normal diffusion ($\alpha = 1$), respectively.

Microswimmers rotated at 19 Hz displayed ballistic behavior at short lag times with high diffusivity constants and α's much greater than 1, indicating superdiffusive behavior.[47] The non-rotating microswimmers displayed linear behavior in each fluid medium, with low generalized diffusivity coefficients and α's close to 1. However, as fluid viscosity increased, the generalized diffusivity of the rotating microswimmers decreased by almost an order of magnitude; this can be seen graphically when all three microswimmers are plotted together in Fig. 3(d), where each microswimmers MSD curve shifted downward in more viscous fluid mediums. The same effect can be seen in the non-rotating microswimmers in Fig. 3(e) and Table I, where the diffusion coefficient decreased as viscosity increased; while the α's also varied in each fluid medium, they were all very close to 1. Non-flagellated microparticles were also examined in Fig. 3(f); while their diffusivities tended to be slightly higher for 30% NaCl and 0.2% methylcellulose, 0.4% methylcellulose showed a negligible difference between microswimmers and microparticles (Table I). The effects of flagellar surface coatings on diffusivity will be explored further in future work.

C. Selected trajectories using feedback control

Directional responsiveness of microswimmers was explored to understand the viability of performing user selected trajectories. A proportional controller was used to change the heading angle, θ, in order to properly align the microswimmer with a desired user selected target destination. The heading angle, θ, was manipulated using the equations

$$\dot{\theta} = k\psi, \tag{5}$$

$$\psi = \phi - \theta, \tag{6}$$

with $\dot{\theta}$ being the time derivative of θ, k being a proportional constant, ψ is the angular difference between the desired angle and the heading angle, and ϕ is the desired angle relative to the microswimmers current position and the target position. For all experiments, in order to reach the desired θ quickly, k was selected to be 5, while the parameters B_s, B_r, $\|\vec{B}\|$, and, ω were fixed throughout the experiments. Figure 4 shows the results of microswimmers performing the trajectories of S, M, and U, the initials of Southern Methodist University, inside a 30% NaCl solution. While the microswimmers do not perform each trajectory perfectly, this was expected due to fluidic disturbances and the constant adjustments being made to θ at a sampling time of 30 frames per second (fps). However, the microswimmers did indeed manage to come close to most of the specified points and ultimately generated the desired shapes. When examining the error from the intended trajectory between the selected points (magenta dots and magenta dashed lines in Fig. 4), the error graphs, shown below each trajectory,
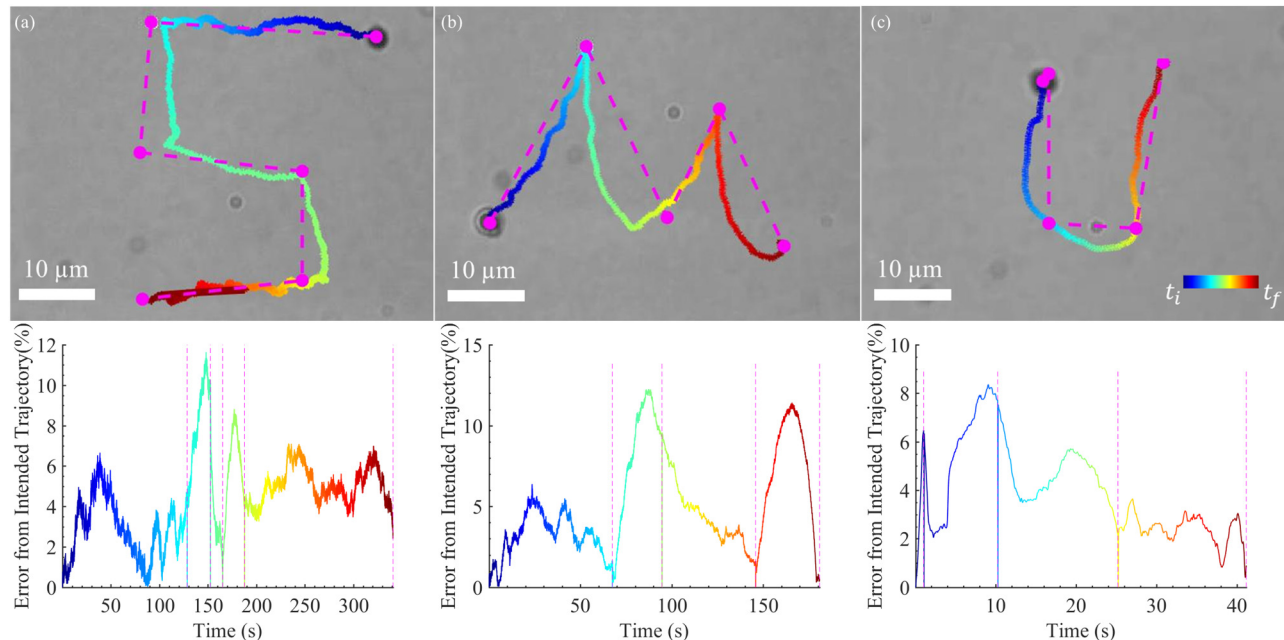
FIG. 4. (a)–(c) User selected path trajectories for S, M, and U. Magenta dots represent the goal position for the microswimmer, while the dashed line represents direct paths between each point. The timings for each trajectory were 360, 180, and 40 s for (a)–(c), respectively. The error from the direct paths between each point and the actual path traversed by the microswimmers can be seen in the graphs beneath each trajectory. Vertical magenta dashed lines in the error plots represent target locations from the respective trajectories.

indicate that the error never exceeded more than 15%, with the microswimmers coming reasonably close to the target positions. Thus, feedback control was achievable and these microswimmers are viable for performing more complex motion tasks in the future.

D. Performance under different rotational handedness

The magnetic dipoles of the microparticles making up each microswimmer always orient themselves to align with the magnetic field vector ($\vec{B}$) in Eq. (1) and propel themselves along the direction vector ($\vec{n}$) in Eq. (2). The dipoles were made to rotate clockwise and counterclockwise in the plane perpendicular to the $\vec{n}$ of each microswimmer by changing the ω from positive to negative [see inset of Fig. 5(a)]. While the performance of microswimmers under the counterclockwise rotation was consistent (and used for all previous experiments) in causing the microswimmers to propel linearly with frequency, the clockwise rotation imparted notably diverse frequency responses between microswimmers. Figures 5(a)–5(d) show the behavior of four microswimmers inside 30% NaCl, examined under both counterclockwise and clockwise rotation, where ω was increased at 1 Hz increments; the microswimmers were first rotated counterclockwise for multiple trials (at least three) and then switched to clockwise rotation for the remaining trials (at least three). In all four cases, the counterclockwise rotation resulted in a linear velocity profile, while the clockwise rotation created anomalous swimming

behavior. In Figs. 5(a) and 5(d), the clockwise rotation resulted in a reduced swimming velocity along the intended direction (positive x-direction), while (b) and (c) resulted in frequency induced reversals of swimming direction (FIRSD),[48] which was repeatable between multiple examinations of these microswimmers. These anomalies and FIRSD effects were determined to be related to the bundling and unbundling of long flagella attached to the microswimmers during the clockwise rotation. Normal form flagella, used throughout these experiments, is naturally left handed and, therefore, has the same sense as a counterclockwise rotating magnetic field. Under a clockwise rotation, however, the flagella are opposite to the sense of the rotating magnetic field, leading to unbundling and reduced motility. For situations with multiple flagella, it has been shown that normal form flagella will naturally bundle together at a rate proportional to the motor frequency,[49] and behave as though they were a single larger flagella, with a thickness equal to the summed radii of the flagella within the bundle[50] [this bundling would explain some of the performance increases seen with the microswimmer in Fig. 5(d) under counterclockwise rotation, while (a)–(c) were all otherwise consistent with predictions of Fig. 2 for 30% NaCl]. While this is not the same kind of bundling experienced by micro-organisms, since they have onboard motors for individual flagella filaments, the bundling of flagella attached to artificial nanoswimmers has been reported previously, with notable performance variations before and after bundling.[33] Using a Nikon Eclipse Ti inverted fluorescence microscope
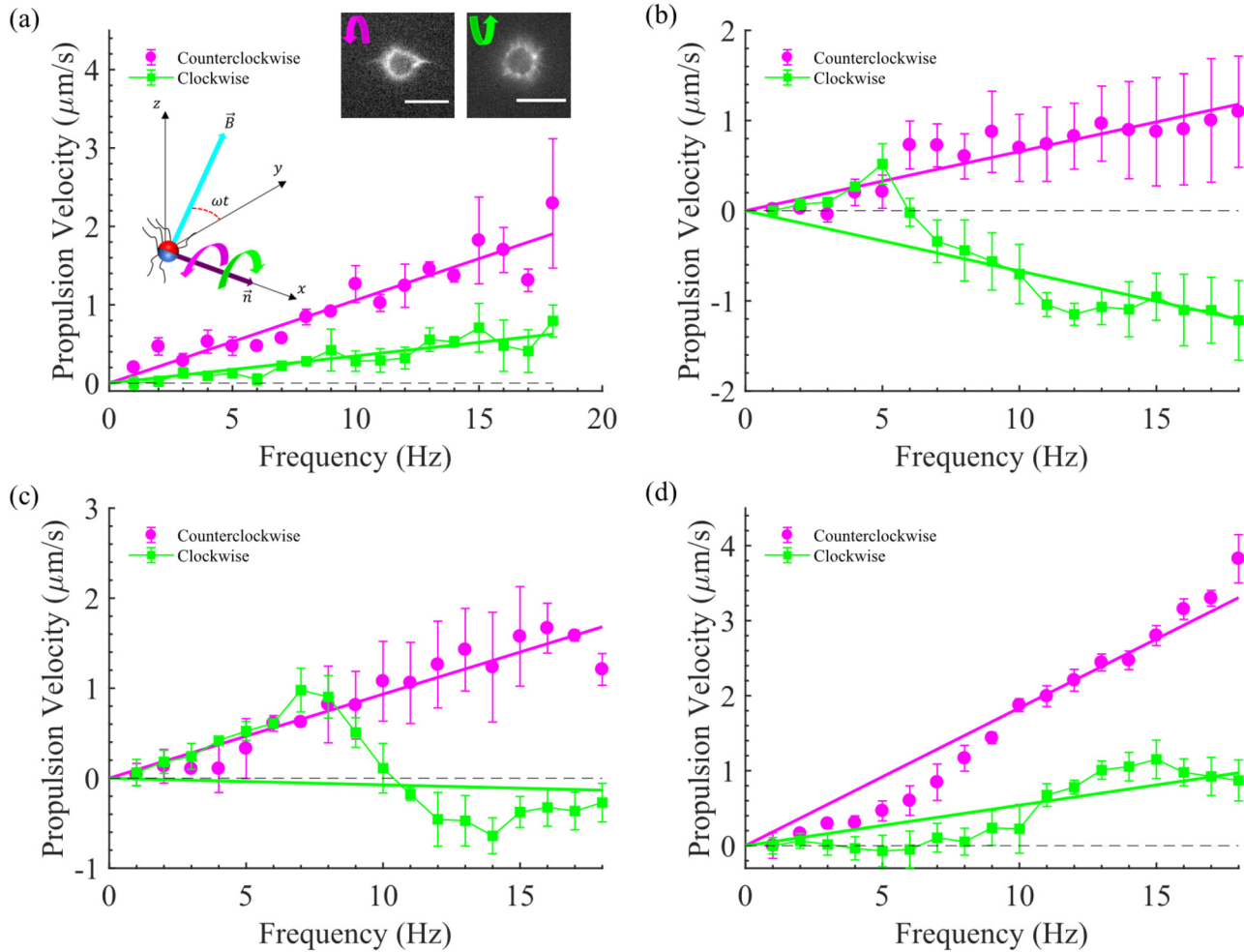
FIG. 5. (a)–(d) Individual microswimmer performance under both counterclockwise and clockwise rotations. The inset of (a) shows how microswimmers interact with magnetic fields produced from Eqs. (1) and (2), where $\vec{B}$ rotates around the x-axis, $\vec{n}$ is the direction vector, red and blue hemispheres represent magnetic dipoles, and the magenta and green arrows represent counterclockwise and clockwise rotation, respectively. Fluorescence imaging in the inset of (a) shows that under counterclockwise rotation, flagellar bundling occurs, while under clockwise rotation, the flagella are unbundled; scale bars in both images are $10\,\mu$m. Dashed lines represent the x-intercepts, solid lines represent the fits, error bars represent the standard error, and the lines between clockwise data points were used to guide the eye.

(see Sec. IV) and a magnetic field controller (MagnebotiX, MFG-100-i), microswimmers were actuated close to the substrate under both counterclockwise and clockwise rotation (5 Hz) to observe bundling and unbundling behavior; instantaneous snapshots of these experiments are shown in the inset of Fig. 5(a). From these images, it can be seen that flagellar bundles form under counterclockwise rotation at the front and rear of the microswimmer, but under clockwise rotation, the previously observed bundles were no longer present. While there may be other factors at work, flagellar bundling and unbundling reasonably explains the diverse behavior observed during these experiments. Flagellar bundling behavior and FIRSD effects will be explored further in future work, with the goal of causing reversals to occur at specific frequency values.

III. CONCLUSION

The reliability of heterogeneously flagellated microswimmers inside fluids of different viscosities was demonstrated. Unlike other microswimmers previously developed in the literature, which often rely on complex fabrication techniques, the presented microswimmers were stochastically assembled by mixing biotinylated flagella with avidin-coated microparticles. The assembled microswimmers were capable of performing consistently in various fluid mediums despite their inherent heterogeneous flagellar surface coatings. Microswimmers inside both 30% NaCl and different methylcellulose concentrations were demonstrated to be linearly dependent on applied rotational frequency; however, microswimmers in the 0.2% methylcellulose had to first overcome an initial velocity lag, present

at frequencies below 5 Hz, before being able to maintain a linear velocity profile; this was suspected to be the result of fluid viscosity and hindrances from polymer fibers at these low frequencies. Microswimmers within 0.2% methylcellulose were shown to outperform microswimmers within the 30% NaCl solution at higher rotational frequencies; this kind of performance increase has been observed previously, in polymer fluids of low concentration, by both micro-organisms and artificial microswimmers.[39–44] Microswimmer propulsion was verified to be caused solely by the attachment of flagella, since non-flagellated microparticles displayed no velocity relationship with increasing frequency. Using a two-dimensional mean square displacement (MSD) analysis, both rotating (19 Hz) and non-rotating (0 Hz) microswimmers were observed. Microswimmers had ballistic motion at short time scales and had significantly higher generalized diffusion coefficients than non-rotating microswimmers. The diffusivity of the rotating microswimmers decreased proportionally as the viscosity of the surrounding fluid medium increased. Interestingly, during the non-rotating scenario, microswimmers had reduced diffusivity compared to non-flagellated microparticles, but this will need more dedicated research to fully understand. Based on these results, the flagellar coatings were shown to allow for ballistic behavior under rotation, but hindered the diffusivity of microswimmers when experiencing only purely diffusive behavior (Brownian motion). Microswimmers were demonstrated to perform selected trajectories using proportional feedback control, and while there was some difference in the actual trajectory performed by the microswimmers, the target destinations and desired shapes were still reasonably achieved with minimal error; differences from the desired trajectory were attributed to instabilities in the fluid and the sampling time of the controller. Finally, microswimmers were shown to exhibit diverse behavior under clockwise rotating magnetic fields, with frequency induced reversals of swimming direction (FIRSD) occurring in some microswimmers; flagellar unbundling was identified as the cause for this behavior and visualized using fluorescence microscopy. While these FIRSD effects were not always guaranteed, they did display remarkable repeatability between individual microswimmers. Likewise, the guarantee of a linear velocity relationship to frequency of microswimmers under counterclockwise rotation was also demonstrated. Future work will be dedicated to further visualizing the bundling behavior of artificial microswimmers and comparing them with their bacterial counterparts, as well as continuing to modulate the surface distribution of flagella to initiate more controlled FIRSD effects. Additional polymorphic forms of flagellar will also be analyzed to understand the performance differences of microswimmers induced by the different coil forms.

IV. METHODS

Isolating flagella from *S. typhimurium* (SJW 1103) is a multistep process that produces a concentrated solution of long, repolymerized flagella, which can then be used to construct millions of microswimmers for on demand experimentation. Once isolated and functionalized, the flagella can be stored for months and can be used to create microswimmers in a matter of minutes. The flagella were isolated and repolymerized using methods adapted from Asakuras original procedures.[31,32] An overview of the process can be seen in Figs. 1(a)–1(k) and will be discussed in detail for the majority of this section. First, *S. typhimurium* was cultured in approximately 10 L of a modified Luria–Bertani (LB) broth recipe (1.00% yeast extract, 1.00% tryptone, 0.30% glucose, 0.66% dipotassium phosphate, and 0.03% monopotassium phosphate in percent by weight). After a 12–16 h incubation-shaking process (36 °C, 130 rpm). The culture media was centrifuged at 3500 relative centrifugal force (rcf) for 35 min, where the bacteria in suspension were pelleted to the bottom of the centrifuge tubes; this centrifugal process was then repeated until all the culture media was used. The pelleted bacteria were then resuspended into a 0.01M potassium phosphate buffer (pH 6.5, polymerization buffer) with a 150 mM of NaCl, and concentrated together into a single tube with a final volume of 50 ml. This concentrated solution of bacteria was then vortexed for 20 min to shear the flagella from the bacterial bodies. The concentrated solution was then centrifuged for 15 min at 16 000 rcf, where afterwards the pelleted bacterial bodies were disposed of and the supernatant containing the flagella was transferred to a new tube. The flagellar solution was then centrifuged at 100 000 rcf for 1 h and the flagella were pelleted. The purified flagellar pellet was then resuspended in the polymerization buffer with a final volume of 1.5 ml per pellet; further purifications at 100 000 rcf for 1 h were performed as needed. About 20% of the isolated flagella were taken and mixed with EZ-Link^{TM} NHS-Biotin (Thermo Fisher Scientific, 20217) using the standardized process outlined by Thermo Fisher. After 30 min, the biotin complex was completely bound to the flagella. The solution was then centrifuged at 16 000 rcf for 15 min to remove any excess biotin from the solution. Both the biotinylated and nonbiotinylated flagellar solutions were then placed in a water bath at 65 °C for 10 min; this step depolymerized the flagella into its constituent flagellin monomers. Both solutions were then centrifuged at 150 000 rcf for 1 h to remove any excess proteins or debris. The supernatants containing the monomers were then transferred to new centrifuge tubes. The biotinylated monomers were then introduced into a 2 M sodium phosphate solution of an equal volume (750 μl each) and incubated for 30 min in order to turn the monomers into short flagella (seeding particles). The seeds were then introduced into the nonbiotinylated monomers, in a 1:4 ratio, and uniformly mixed by vortexing for 5 min; they were then left to incubate for 48 h at room temperature. The resulting repolymerized flagella were between 10 and 25 μm in length with one of their end points being biotinylated. The repolymerized flagella were then centrifuged at 10 000 rcf for 1 h and resuspended using a 0.01M potassium phosphate (pH 7.5, conjugation buffer) with 150 mM of NaCl solution for a total volume of 1.5 ml. Cy3 dye (Sigma Aldrich, GEPA23001) was reconstituted in conjugation buffer (1.5 ml) and then mixed in a 1:1 ratio with the flagellar solution. 1 M of sodium bicarbonate was added (5% of the final volume) to help the dye attach to the flagella.

After 2 h, the Cy3 labeled flagella were centrifuged at 100 000 rcf and resuspended using the conjugation buffer to a total volume of 1.5 ml. Approximately 20 μl of flagellar solution was then placed in a 5 ml centrifuge tube. Avidin-coated particles 2 μm in diameter (Spherotech, SVFM-20-5), in a 1 μl solution, were introduced into the centrifuge tube and gently shaken for 30 min to ensure microswimmer formation. Avidin–biotin bonding, between the microparticle and the flagellar ends, is the strongest non-covalent bond found in

nature. The solution was then diluted with the experimental fluid (saline or methylcellulose solution) until the total volume was 3 ml. Using a Nikon Eclipse Ti inverted fluorescence microscope, the microswimmers were visualized to ensure flagellar attachment using a 100× objective and an electron-multiplying charge-coupled device (EMCCD) camera (iXon 897, Andor Technology). Entire surfaces of the microswimmers were usually coated with flagella; however, lengths of the individual attached flagellar filaments varied. The average length of flagella was estimated to be about 8 μm; the length reduction was the result of flagella shearing from centrifugation and pipetting. The microswimmers were then loaded into a circular poly-dimethylsiloxane (PDMS) chamber, approximately 2 mm in diameter and 1 mm in height, on top of a No. 1.5 coverslip. The chamber was sealed at the top with another coverslip in order to limit evaporation and minimize internal flows. The chamber was then loaded into a custom-built triaxial approximate Helmholtz coil system situated on top of a Leica DM IRB inverted microscope (type 090-132.701). A 63× objective and a complementary metal oxide semiconductor (CMOS) camera (Point Grey, FL3-U3-13Y3M-C) recording at 30 frames per second (fps) were used to visualize and capture data from the experiments. Programmable power supplies (KEPCO-BOP-5M) were linked to a data acquisition board (National Instruments, DAQ) and interfaced with a customized LabVIEW program to control coil output signals. A visual description of this system layout can be found in Fig. 1(p). Once the sample was given enough time to settle (internal flows dissipate), stationary microswimmers were located in the solution and tested to understand their response to increasing rotational magnetic field frequency. The magnetic fields produced by the approximate Helmholtz coil system were designed such that the magnetic field increased proportionally to the rotational magnetic field frequency ($B_r = 0.5\omega$); this was done to ensure microswimmers followed the rotating field and did not desynchronize.[51] The magnetic field strengths and other experimental variables for each test were recorded through LabVIEW and exported to an Excel spreadsheet. The LabVIEW program was also integrated with the proportional controller, able to retroactively track a microswimmer and guide it to a user selected point of interest. MATLAB was used to analyze the collected data and produce the plots and figures found in this manuscript. Component velocity data were collected at 30 fps, and the change in position of the microswimmer along the positive x-direction was calculated between each frame to produce the velocity; velocity was averaged over the time intervals spent in each rotational frequency. The pixel distance was found to be 0.152 μm/pixel, with the camera resolution being 512 × 640. For more information regarding the approximate Helmholtz coil system, readers are encouraged to refer to Refs. 21,22,31,33,34,52. Microswimmers were tested in three different fluidic environments: a saline solution and two methylcellulose solutions. The saline solution was created by mixing de-ionized water and NaCl (Sigma Aldrich, S5886) into a 30% concentration. Methylcellulose (Sigma Aldrich, M0512) at 0.2% and 0.4% concentrations were synthesized using directions provided by Sigma Aldrich.

Fittings for mean square displacement graphs (Fig. 3) were calculated using a delayed rejection adaptive Metropolis (DRAM) Markov chain Monte Carlo algorithm.[46] Markov chains had a length of 50 000 and only the last 10% of the chain was used to estimate the parameters shown in Table I. A burn-in of 10 000 was used before adaptation occurred using the DRAM process. No prior distributions or limits were placed on the algorithm as it calculated the parameters for Eq. (4). The range of data used in the algorithm was 1/30th to 3 s for the non-rotating experiments and 2–5 s for the rotating experiments. The MSD data for 0.2% methylcellulose microswimmer in Fig. 3(e) and the 30% NaCl microparticle in Fig. 3(f) used a modified mean square displacement analysis in order to remove small internal flows; the process outlined in the literature[53] was implemented to equate the start position with the end position. Aside from these two cases, the MSD analysis outlined in Sec. II B was uniformly applied.

REFERENCES

[1] E. M. Purcell, Am. J. Phys. **45**, 3 (1977).
[2] E. Lauga and T. R. Powers, Rep. Progress Phys. **72**, 096601 (2009).
[3] A. Selimis, V. Mironov, and M. Farsari, Microelectron. Eng. **132**, 83 (2015).
[4] U. Bozuyuk, O. Yasa, I. C. Yasa, H. Ceylan, S. Kizilel, and M. Sitti, ACS Nano **12**, 9617 (2018).
[5] S. Kim, F. Qiu, S. Kim, A. Ghanbari, C. Moon, L. Zhang, B. J. Nelson, and H. Choi, Adv. Mater. **25**, 5863 (2013).
[6] F. Qiu, R. Mhanna, L. Zhang, Y. Ding, S. Fujita, and B. J. Nelson, Sens. Actuators B Chem. **196**, 676 (2014).
[7] F. Qiu, L. Zhang, K. E. Peyer, M. Casarosa, A. Franco-Obregón, H. Choi, and B. J. Nelson, J. Mater. Chem. B **2**, 357 (2014).
[8] A. Servant, F. Qiu, M. Mazza, K. Kostarelos, and B. J. Nelson, Adv. Mater. **27**, 2981 (2015).
[9] M. Suter, L. Zhang, E. C. Siringil, C. Peters, T. Luehmann, O. Ergeneman, K. E. Peyer, B. J. Nelson, and C. Hierold, Biomed. Microdevices **15**, 997 (2013).
[10] S. Tottori, L. Zhang, F. Qiu, K. K. Krawczyk, A. Franco-Obregón, and B. J. Nelson, Adv. Mater. **24**, 811 (2012).
[11] L. Zhang, J. J. Abbott, L. Dong, B. E. Kratochvil, D. Bell, and B. J. Nelson, Appl. Phys. Lett. **94**, 064107 (2009).
[12] L. Zhang, K. E. Peyer, and B. J. Nelson, Lab Chip **10**, 2203 (2010).
[13] X. Wang, X. Qin, C. Hu, A. Terzopoulou, X. Chen, T. Huang, K. Maniura–Weber, S. Pané, and B. J. Nelson, Adv. Funct. Mater. **28**, 1804107 (2018).
[14] W. Gao, X. Feng, A. Pei, C. R. Kane, R. Tam, C. Hennessy, and J. Wang, Nano Lett. **14**, 305 (2013).
[15] K. Kamata, Z. Piao, S. Suzuki, T. Fujimori, W. Tajiri, K. Nagai, T. Iyoda, A. Yamada, T. Hayakawa, M. Ishiwara *et al.*, Sci. Rep. **4**, 4919 (2014).
[16] X. Yan, Q. Zhou, M. Vincent, Y. Deng, J. Yu, J. Xu, T. Xu, T. Tang, L. Bian, Y.-X. J. Wang *et al.*, Sci. Rob. **2**, eaaq1155 (2017).
[17] I. S. Khalil, A. Fatih Tabak, A. Klingner, and M. Sitti, Appl. Phys. Lett. **109**, 033701 (2016).
[18] K. E. Peyer, E. C. Siringil, L. Zhang, M. Suter, and B. J. Nelson, in *Conference on Biomimetic and Biohybrid Systems* (Springer, 2013), pp. 216–227.
[19] L. Baraban, D. Makarov, R. Streubel, I. Monch, D. Grimm, S. Sanchez, and O. G. Schmidt, ACS Nano **6**, 3383 (2012).

[20]S. Das, E. B. Steager, M. A. Hsieh, K. J. Stebe, and V. Kumar, J. Micro-Bio Rob. **14**, 25 (2018).

[21]U. K. Cheang, H. Kim, D. Milutinović, J. Choi, L. Rogowski, and M. J. Kim, in *12th International Conference on Ubiquitous Robots and Ambient Intelligence (URAI)* (IEEE, 2015), pp. 518–523.

[22]U. K. Cheang and M. J. Kim, J. Nanopart. Res. **17**, 145 (2015).

[23]M. Kaynak, A. Ozcelik, A. Nourhani, P. E. Lammert, V. H. Crespi, and T. J. Huang, Lab Chip **17**, 395 (2017).

[24]H. C. Berg, Nature **254**, 389 (1975).

[25]K. Hasegawa, H. Suzuki, F. Vonderviszt, Y. Mimori-Kiyosue, and K. Namba, Nat. Struct. Biol. **5**, 125 (1998).

[26]F. Hayashi, H. Tomaru, E. Furukawa, K. Ikeda, H. Fukano, and K. Oosawa, J. Bacteriol. **195**, 3503 (2013).

[27]R. Kamiya and S. Asakura, J. Mol. Biol. **108**, 513 (1976).

[28]N. C. Darnton and H. C. Berg, Biophys. J. **92**, 2230 (2007).

[29]R. Kamiya and S. Asakura, J. Mol. Biol. **106**, 167 (1976).

[30]T. Qiu, T.-C. Lee, A. G. Mark, K. I. Morozov, R. Münster, O. Mierka, S. Turek, A. M. Leshansky, and P. Fischer, Nat. Commun. **5**, ncomms6119 (2014).

[31]S. Asakura, G. Eguchi, and T. Iino, J. Mol. Biol. **10**, 42 (1964).

[32]S. Asakura, G. Eguchi, and T. Iino, J. Mol. Biol. **35**, 227 (1968).

[33]J. Ali, U. K. Cheang, J. D. Martindale, M. Jabbarzadeh, H. C. Fu, and M. J. Kim, Sci. Rep. **7**, 14098 (2017).

[34]J. Ali, U. K. Cheang, A. Darvish, H. Kim, and M. J. Kim, APL Mater. **5**, 116106 (2017).

[35]U. K. Cheang and M. J. Kim, Appl. Phys. Lett. **109**, 034101 (2016).

[36]R. Moreira, F. Chenlo, C. Silva, and M. D. Torres, LWT **84**, 764 (2017).

[37]P. Nasatto, F. Pignon, J. Silveira, M. Duarte, M. Noseda, and M. Rinaudo, Polymers **7**, 777 (2015).

[38]Z. Hai-Lang and H. Shi-Jun, J. Chem. Eng. Data **41**, 516 (1996).

[39]E. E. Riley and E. Lauga, Europhys. Lett. **108**, 34003 (2014).

[40]D. Schamel, A. G. Mark, J. G. Gibbs, C. Miksch, K. I. Morozov, A. M. Leshansky, and P. Fischer, ACS Nano **8**, 8794 (2014).

[41]J. Teran, L. Fauci, and M. Shelley, Phys. Rev. Lett. **104**, 038101 (2010).

[42]H. C. Fu, T. R. Powers, and C. W. Wolgemuth, Phys. Rev. Lett. **99**, 258101 (2007).

[43]E. Lauga, Phys. Fluids **19**, 083104 (2007).

[44]H. C. Berg and L. Turner, Nature **278**, 349 (1979).

[45]X. Michalet, Phys. Rev. E **82**, 041914 (2010).

[46]H. Haario, M. Laine, A. Mira, and E. Saksman, Stat. Comput. **16**, 339 (2006).

[47]Y.-F. Chen, H.-H. Wei, Y.-J. Sheng, and H.-K. Tsao, Phys. Rev. E **93**, 042611 (2016).

[48]F. Bachmann, K. Bente, A. Codutti, and D. Faivre, Phys. Rev. Appl. **11**, 034039 (2019).

[49]M. Kim, J. C. Bird, A. J. Van Parys, K. S. Breuer, and T. R. Powers, Proc. Natl. Acad. Sci. U.S.A. **100**, 15481 (2003).

[50]M. J. Kim, M. J. Kim, J. C. Bird, J. Park, T. R. Powers, and K. S. Breuer, Exp. Fluids **37**, 782 (2004).

[51]U. K. Cheang, F. Meshkati, H. Kim, K. Lee, H. C. Fu, and M. J. Kim, Sci. Rep. **6**, 30472 (2016).

[52]J. Ali, U. K. Cheang, Y. Liu, H. Kim, L. Rogowski, S. Sheckman, P. Patel, W. Sun, and M. J. Kim, AIP Adv. **6**, 125205 (2016).

[53]J. W. Mellnik, M. Lysy, P. A. Vasquez, N. S. Pillai, D. B. Hill, J. Cribb, S. A. McKinley, and M. G. Forest, J. Rheol. **60**, 379 (2016).